A Rotational and Irrotational Flow Past a Slender Body of Revolution in a Tube

A Rotational and an Irrotational Flow Past a Slender Body of Revolution in a Tube

Hitoshi NAKATANI* and Yoshihiro MIYAI*

(Received June 15, 1975)

Abstract

A rotational and an irrotational flow past a slender body of revolution located on the axis of an infinitely long tube of constant diameter are analyzed using a slender body in slender tube theory. That is, three different types of flow are considered as the condition of flow; (1) irrotational flow, (2) rotational flow with a paraboloidal velocity distribution far upstream, (3) swirling flow with constant axial and angular velocities far upstream.

From these results, surface pressure coefficients and stream lines past a slender body of revolution are calculated. Next, in the case of (1) and (2), a comparison is made between these analytic results and other numerical results calculated from the distribution of the finite number of doublets for a slender ellipsoid of revolution. Then, the range of the validity of a slenderness ratio is examined in the case of (1).

1. Introduction

A case of a steady, incompressible flow past an axisymmetric body of revolution located on the axis of an infinitely long tube of constant diameter is considered. A rotational flow past a sphere in a tube has already been analyzed by Wei Lai[1]. His analysis was based on a vortex sheet over one segment of a diameter of the sphere. It is not easy to find the function which represents this vortex sheet. However, if a body and a tube are slender, an approximate solution of closed form may be obtained. The corresponding theory is known as the slender body in slender tube theory for the flow past a body of revolution.

In this paper, three different types of flow are considered; (1) irrotational flow, (2) rotational flow with a paraboloidal velocity distribution far upstream and (3) swirling flow with constant axial and angular velocities far upstream.

Surface pressure coefficients and flow patterns can be obtained for these types of flow. Besides, the difference between the irrotational flow and the rotational flow are examined from surface pressure coefficients, and the range of the validity of a slenderness ratio is examined.

2. Basic Equation and Boundary Conditions

Cylindrical co-ordinates (x, r, θ) will be used as shown in Fig. 1.

* Department of Mechanical Engineering, College of Engineering.

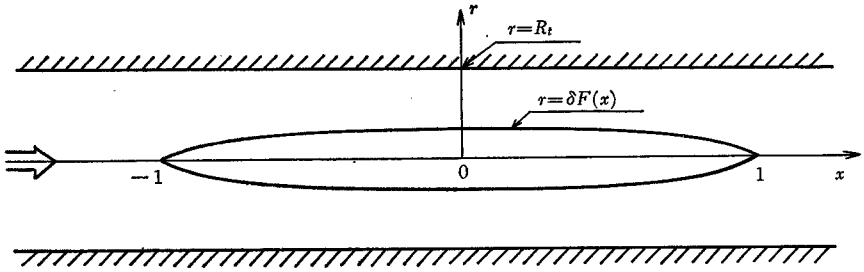

Fig. 1. Co-ordinate system for a body of revolution in a tube

Let lengths be normalized against the half length of the body.

The differential equation for the Stokes' stream function $\Psi(x, r)$ of an axisymmetric incompressible flow may be written as follows according to Wei Lai[1] or Batchelor.[2]

$$\frac{\partial^2\Psi}{\partial x^2}+\frac{\partial^2\Psi}{\partial r^2}-\frac{1}{r}\frac{\partial\Psi}{\partial r}=r^2\frac{dH}{d\Psi}-\frac{1}{2}\frac{df}{d\Psi}, \tag{1}$$

where $H(\Psi)$ and $f(\Psi)$ are to be determined from the conditions far upstream. The velocity components are

$$u=-\frac{1}{r}\frac{\partial\Psi}{\partial x}, \qquad w=\frac{1}{r}\frac{\partial\Psi}{\partial r}. \tag{2}$$

The shape of a slender body of revolution is

$$r=\delta F(x), \quad -1<x<1, \quad F(-1)=F(1)=0, \quad F_{max}=1, \tag{3}$$

where, δ is a small parameter measuring the relative slenderness of a family of bodies whose shape function is $F(x)$ (see Fig. 1).

The inner radius of an infinitely long tube is

$$r=R_t, \quad (R_t=\text{const.}). \tag{4}$$

The boundary condition on the slender body of revolution is

$$\Psi|_{r=\delta F(x)}=0. \tag{5}$$

The boundary condition on the tube wall is

$$\Psi|_{r=R_t}=\text{const.}. \tag{6}$$

3. Basic Equations and Boundary Conditions for Each Flow Field

Case 1. The upstream conditions in this case are characterized by

$$w=U_\infty \text{ (const.)}, \quad u=v=0.$$

Thus

$$\Psi_\infty=\frac{1}{2}r^2U_\infty, \quad H(\Psi)=f(\Psi)=0. \tag{7}$$

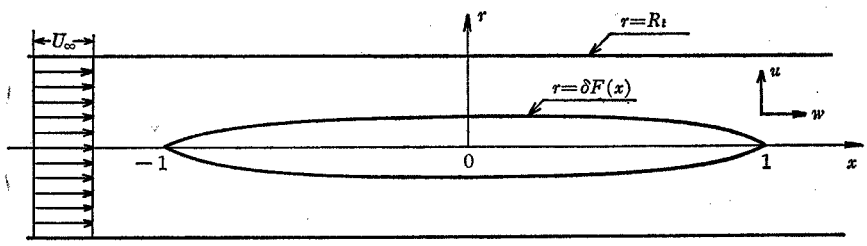

Fig. 2. Irrotational flow past a slender body of revolution in a tube

The governing equation is

$$\frac{\partial^2\Psi}{\partial x^2}+\frac{\partial^2\Psi}{\partial r^2}-\frac{1}{r}\frac{\partial\Psi}{\partial r}=0. \tag{8}$$

Boundary conditions are obtained from Eqs. (5) and (6), that is,

$$\Psi|_{r=\delta F(x)}=0, \qquad \Psi|_{r=R_t}=\Psi_\infty|_{r=R_t}=\frac{1}{2}R_t^2U_\infty\,. \tag{9}$$

Case 2. The upstream conditions are characterized by

$$w=W\left(1-\frac{r^2}{R_t^2}\right), \qquad u=v=0.$$

Thus

$$\Psi_\infty=W\left(\frac{1}{2}r^2-\frac{r^4}{4R_t^2}\right), \quad H(\Psi)=\frac{1}{2}W^2-\frac{2W\Psi}{R_t^2}, \quad f(\Psi)=0. \tag{10}$$

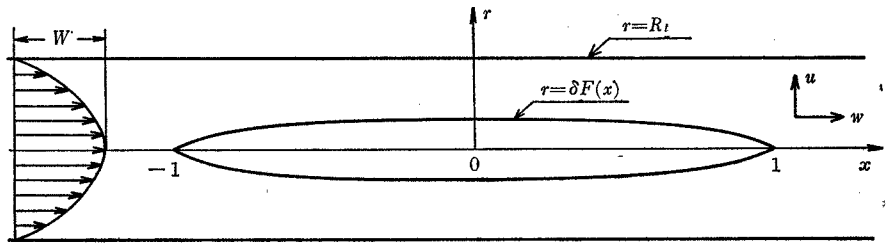

Fig. 3. Rotational flow with a paraboloidal velocity distribution far upstream past a slender body of revolution in a tube

The governing equation is

$$\frac{\partial^2\Psi}{\partial x^2}+\frac{\partial^2\Psi}{\partial r^2}-\frac{1}{r}\frac{\partial\Psi}{\partial r}=-2W\frac{r^2}{R_t^2}\,. \tag{11}$$

Boundary conditions are obtained from Eqs. (5) and (6), that is

$$\Psi|_{r=\delta F(x)}=0, \qquad \Psi|_{r=R_t}=\Psi_\infty|_{r=R_t}=\frac{1}{2}R_t^2W. \tag{12}$$

Case 3. The upstream conditions are characterized by

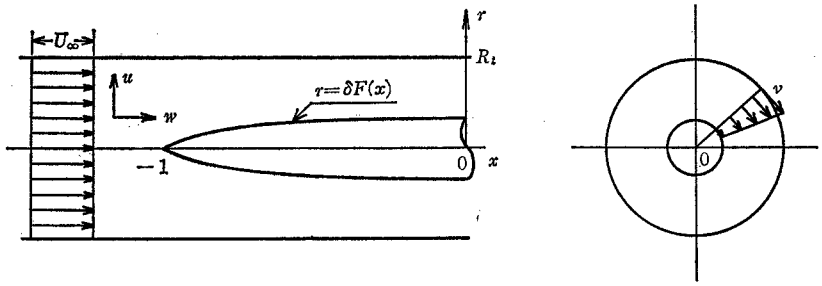

Fig. 4. Swirling flow far upstream past a slender body of revolution in a tube

$$\left.\begin{aligned} &w=U_\infty \text{ (const.)}, \quad u=0, \quad v/r=\omega \text{ (const.)}. \\ &\text{Thus} \\ &\Psi_\infty=\frac{1}{2}r^2U_\infty, \quad f(\Psi)=r^2v^2=\sigma^2\Psi^2 \\ &\text{where } \sigma, \text{ the reciprocal of a Rossby number, is } 2\omega/U_\infty, \\ &H(\Psi)=\frac{1}{2}(U_\infty^2+v^2)+\frac{1}{2}v^2, \\ &\text{and} \\ &\frac{dH}{d\Psi}=\frac{d}{d\Psi}v^2=\frac{1}{2}\sigma^2U_\infty . \end{aligned}\right\} \tag{13}$$

The governing equation is

$$\frac{\partial^2\Psi}{\partial x^2}+\frac{\partial^2\Psi}{\partial r^2}-\frac{1}{r}\frac{\partial\Psi}{\partial r}+\sigma^2\Psi=\frac{1}{2}\sigma^2r^2U_\infty^2 . \tag{14}$$

Boundary conditions are also obtained from Eqs. (5) and (6), that is,

$$\Psi|_{r=\delta F(x)}=0, \quad \Psi|_{r=R_t}=\Psi_\infty|_{r=R_t}=\frac{1}{2}R_t^2U_\infty . \tag{15}$$

Next, let U_∞ be unity and the mass flux far upstream for each flow field be constant, then, W in case (2) becomes 2 (see Figs. 2, 3 and 4).

4. Analysis

Case 1. We now rewrite the problem in terms of a perturbation field due to the body. Let us denote by $\psi(x, r)$ the perturbation stream function. We then have

$$\Psi(x, r)=\Psi_\infty(x, r)+\psi(x, r). \tag{16}$$

The differential equation (8) then takes the form

$$\frac{\partial^2\psi}{\partial x^2}+\frac{\partial^2\psi}{\partial r^2}-\frac{1}{r}\frac{\partial\psi}{\partial r}=0 . \tag{17}$$

Next, the transformation given by Cole[3] is used for r, that is,

$$r^*=\frac{r}{\delta}, \tag{18}$$

and the perturbation stream function $\psi(x, r)$ is expanded in the following form:

$$\psi(x, r)=\mu_0(\delta)\psi_0(x, r^*)+\mu_1(\delta)\psi_1(x, r^*)+\mu_2(\delta)\psi_2(x, r^*)+\cdots\cdots\cdots. \tag{19}$$

Approximate equations for each order term result from equating the coefficients of like powers of $(\delta^2)^n$ in Eqs. (17), (18) and (19), considering $\mu_0(\delta)=\delta^2$, $\mu_1(\delta)=\delta^4$, $\mu_2(\delta)=\delta^6$, ····· :

$$O(\delta^2): \quad \psi_{0r^*r^*}-\frac{1}{r^*}\psi_{0r^*}=0, \tag{20}$$

$$O(\delta^4): \quad \psi_{1r^*r^*}-\frac{1}{r^*}\psi_{1r^*}+\psi_{0xx}=0, \tag{21}$$

$$O(\delta^6): \quad \psi_{2r^*r^*}-\frac{1}{r^*}\psi_{2r^*}+\psi_{1xx}=0. \tag{22}$$

Besides, boundary conditions for each order term are given from Eqs. (4), (16), (18) and (19) as follows:

$$O(\delta^2): \quad (\Psi_\infty+\psi_0)|_{r^*=F(x)}=0, \qquad \psi_0|_{r^*=R_t^*}=0, \tag{23}$$

$$O(\delta^4): \quad \psi_1|_{r^*=F(x)}=0, \qquad \psi_1|_{r^*=R_t^*}=0, \tag{24}$$

$$O(\delta^6): \quad \psi_2|_{r^*=F(x)}=0, \qquad \psi_2|_{r^*=R_t^*}=0. \tag{25}$$

Let us obtain the approximate solutions for each order term from the above approximate equations and the boundary conditions. The solution of Eq. (20) is

$$\psi_0(x, r^*)=C_1(x)+C_2(x)r^{*2}. \tag{26}$$

The unknown functions $C_1(x)$ and $C_2(x)$ are determined from the boundary conditions as follows:

$$C_1(x)=-\frac{R_t^{*2}\alpha(x)}{2\{1-\alpha(x)\}}U_\infty, \qquad C_2(x)=\frac{\alpha(x)}{2\{1-\alpha(x)\}}U_\infty.$$

where

$$\alpha(x)=\frac{F(x)^2}{R_t^{*2}} \text{ (local blockage ratio).}$$

Thus, the solution for $\psi_0(x, r^*)$ is

$$\psi_0(x, r^*)=\frac{R_t^{*2}\alpha(x)}{2\{1-\alpha(x)\}}U_\infty\left[\frac{r^{*2}}{R_t^{*2}}-1\right]=A_0(x)\left[\frac{r^{*2}}{R_t^{*2}}-1\right], \tag{27}$$

where

$$A_0(x)=R_t^{*2}\alpha(x)U_\infty/[2\{1-\alpha(x)\}].$$

Next, substituting Eq. (27) into Eq. (21),

$$\frac{\partial^2\psi_1}{\partial r^{*2}}-\frac{1}{r^*}\frac{\partial\psi_1}{\partial r^*}=-A_0''(x)\left[\frac{r^{*2}}{R_t^{*2}}-1\right]. \tag{28}$$

Substituting $\psi_1(x, r^*)=r^*\psi_1^*(x, r^*)$ into the left side hand of Eq. (28) and rearranging

this equation, the following operator is obtained:

$$\frac{1}{r^*}\left\{\frac{\partial}{\partial r^*}\left(r^{*2}\frac{\partial}{\partial r^*}-r^*\right)\right\}. \tag{29}$$

Using this operator, Eq. (28) is rewritten as follows:

$$\begin{aligned}
&\frac{\partial}{\partial r^*}\left(r^{*2}\frac{\partial\psi_1^*}{\partial r^*}-r^*\psi_1^*\right)=r^*A_0''(x)\left[1-\frac{r^{*2}}{R_t^{*2}}\right],\\
&r^{*2}\frac{\partial\psi_1^*}{\partial r^*}-r^*\psi_1^*=A_0''(x)\left[\frac{r^{*2}}{2}-\frac{r^{*4}}{4R_t^{*2}}\right]+D_1(x),\\
&\frac{\partial\psi_1^*}{\partial r^*}-\frac{1}{r^*}\psi_1^*=A_0''(x)\left[\frac{1}{2}-\frac{r^{*2}}{4R_t^{*2}}\right]+\frac{D_1(x)}{r^{*2}}.
\end{aligned} \tag{30}$$

Then, from the linear differential equation (30), the solution for $\psi_1^*(x, r^*)$ is given by

$$\begin{aligned}
&\psi_1^*(x,r^*)=e^{\int\frac{1}{r^*}dr^*}\left\{\int\left[A_0''(x)\left(\frac{1}{2}-\frac{r^{*2}}{4R_t^{*2}}\right)+\frac{D_1(x)}{r^{*2}}\right]e^{-\int\frac{1}{r^*}dr^*}dr^*+D_2(x)\right\},\\
&\psi_1^*(x,r^*)=\frac{A_0''(x)}{2}r^*\log r^*-\frac{A''_0(x)}{8}\frac{r^{*3}}{R_t^{*2}}-\frac{D_1(x)}{r^*}+r^*D_2(x),\\
&\psi_1(x,r^*)=r^*\psi_1(x,r^*)=D_1(x)+D_2(x)r^{*2}+\frac{A_0''(x)}{2}r^{*2}\log r^*-\frac{A_0''(x)}{8}\frac{r^{*4}}{R_t^{*2}}.
\end{aligned} \tag{31}$$

The unknown functions $D_1(x)$ and $D_2(x)$ are determined from the boundary conditions, that is,

$$\begin{aligned}
&D_1(x)=-\frac{A_0''(x)}{8}F(x)^2-\frac{A_0''(x)}{4}\frac{F(x)^2}{\{1-\alpha(x)\}}\log\alpha(x),\\
&D_2(x)=\frac{A''_0(x)}{8}\{1+\alpha(x)\}-\frac{A_0''(x)}{2}\frac{1}{\{1-\alpha(x)\}}\{\log R_t^*-\alpha(x)\log F(x)\}.
\end{aligned}$$

Similary, from Eq. (22), the solution for $\psi_2(x, r^*)$ is given by

$$\begin{aligned}
\psi_2(x,r^*)=&E_1(x)+E_2(x)r^{*2}-\frac{D_2''(x)}{8}r^{*4}-\frac{D_1''(x)}{2}r^{*2}\log r^*\\
&-\frac{A_0^{(4)}(x)}{16}\left(r^{*4}\log r^*-\frac{3}{4}r^{*4}\right)+\frac{A_0^{(4)}(x)}{192}\frac{r^{*6}}{R_t^{*2}},
\end{aligned}$$

where

$$\begin{aligned}
E_1(x)=&-\frac{D_2''(x)}{8}R_t^{*2}F(x)^2+\frac{D_1''(x)}{4}\frac{F(x)^2\log\alpha(x)}{1-\alpha(x)}\\
&-\frac{A_0^{(4)}(x)}{16}F(x)^2R_t^{*2}\frac{\log R_t^*-\alpha(x)\log F(x)}{1-\alpha(x)}+\frac{A_0^{(4)}(x)}{12}F(x)^2R_t^{*2}\\
&+\frac{A_0^{(4)}(x)}{192}F(x)^2\{1-\alpha(x)\},
\end{aligned}$$

$$E_2(x)=\frac{D_2''(x)}{8}R_t^{*2}\{1+\alpha(x)\}+\frac{D_1''(x)}{2}\frac{\log R_t^*-\alpha(x)\log\alpha(x)}{1-\alpha(x)}$$
$$-\frac{A_0^{(4)}(x)}{16}R_t^{*2}\frac{1-\alpha(x)^2\log F(x)}{1-\alpha(x)}-\frac{3}{64}A_0^{(4)}(x)R_t^{*2}\{1+\alpha(x)\}$$
$$-\frac{A_0^{(4)}(x)}{192}R_t^{*2}\{1+\alpha(x)+\alpha(x)^2\}\ .$$

Thus, $\Psi(x, r)$ is summarized as follows:

$$\Psi(x, r)=\delta^2\left\{\frac{1}{2}r^{*2}U_\infty+\psi_0(x, r^*)\right\}+\delta^4\psi_1(x, r^*)+\delta^6\psi_2(x, r^*)+\cdots\cdots\ . \tag{32}$$

Case 2. Substituting Eq. (16) into Eq. (11), the same differential equation (17) as in *case* 1 is obtained, that is,

$$\frac{\partial^2\psi}{\partial x^2}+\frac{\partial^2\psi}{\partial r^2}-\frac{1}{r}\frac{\partial\psi}{\partial r}=0\ . \tag{33}$$

Next, to obtain approximate solutions, using the transformation for r given by Eq. (18) and substituting Eq. (19) into Eq. (33), the same approximate equations for each order term as Eqs. (20) and (21) in *case* 1 are obtained. The boundary conditions are also the same as Eq. (23) and (24). Therefore, approximate solutions $\psi_i(x, r^*)$ for each order term are as follows:

$$O(\delta^2):\ \psi_0(x, r^*)=A_1(x)\left[\frac{r^{*2}}{R_t^{*2}}-1\right], \tag{34}$$

where

$$A_1(x)=\frac{R_t^{*2}\alpha(x)W}{2\{1-\alpha(x)\}}\left\{1-\frac{1}{2}\alpha(x)\right\}.$$

$$O(\delta^4);\ \psi_1(x, r^*)=D_3(x)+D_4(x)r^{*2}+\frac{A_1''(x)}{2}r^{*2}\log r^*-\frac{A_1''(x)}{8}\frac{r^{*4}}{R_t^{*2}}\ , \tag{35}$$

where

$$D_3(x)=-\frac{A_1''(x)}{8}F(x)^2-\frac{A_1''(x)}{4}\frac{F(x)^2}{1-\alpha(x)}\log\alpha(x)\ ,$$

$$D_4(x)=\frac{A_1''(x)}{8}\{1+\alpha(x)\}-\frac{A_1''(x)}{2}\frac{1}{1-\alpha(x)}\{\log R_t^*-\alpha(x)\log F(x)\}\ .$$

$\Psi(x, r)$ is summarized as follows:

$$\Psi(x, r)=\delta^2\left[W\left(\frac{1}{2}r^{*2}-\frac{r^{*4}}{4R_t^{*2}}\right)+\psi_0(x, r^*)\right]+\delta^4\psi_1(x, r^*)+\cdots\cdots\ . \tag{36}$$

Case 3. Substituting Eq. (16) into Eq. (14), the differential equation for $\psi(x, r)$ is given as follows:

$$\frac{\partial^2\psi}{\partial x^2}+\frac{\partial^2\psi}{\partial r^2}-\frac{1}{r}\frac{\partial\psi}{\partial r}+\sigma^2\psi=0\ . \tag{37}$$

Using the transformation for r in Eq. (18) and substituting Eq. (19) into Eq. (37), approximate equations for each order term are as follows:

$$O(\delta^2):\ \psi_{0r^*r^*}-\frac{1}{r^*}\psi_{0r^*}=0\,, \tag{38}$$

$$O(\delta^4):\ \psi_{1r^*r^*}-\frac{1}{r^*}\psi_{1r^*}+\psi_{0xx}+\sigma^2\psi_0=0\,. \tag{39}$$

The boundary conditions are of the same form as in *case* 1 and in *case* 2.

Let us obtain the approximate solutions for each order term from the above approximate equations and the boundary conditions. As the governing equation and the boundary conditions for $O(\delta^2)$ are of the same form as those in *case* 1, the approximate solution for $O(\delta^2)$ is of the same form as that in *case* 1, that is,

$$\psi_0(x, r^*)=A_0(x)\left[\frac{r^{*2}}{R_t^{*2}}-1\right],$$

where

$$A_0(x)=R_t^{*2}\alpha(x)U_\infty/[2\{1-\alpha(x)\}]\,.$$

Next, the solution for $\psi_1(x, r^*)$ is given from Eq. (39) as follows:

$$\psi_1(x, r^*)=D_5(x)+D_6(x)r^{*2}-\{\sigma^2A_0(x)-A_0''(x)\}\left(\frac{1}{2}r^{*2}\log r^*-\frac{1}{8}\frac{r^{*4}}{R_t^{*2}}\right).$$

The unknown functions $D_5(x)$ and $D_6(x)$ are determined from the boundary conditions, that is,

$$D_5(x)=\{\sigma^2A_0(x)-A_0''(x)\}\left[\frac{F(x)^2\log\alpha(x)}{4\{1-\alpha(x)\}}+\frac{1}{8}F(x)^2\right],$$

$$D_6(x)=\{\sigma^2A_0(x)-A_0''(x)\}\left[\frac{\log R_t^*-\alpha(x)\log F(x)}{2\{1-\alpha(x)\}}-\frac{1}{8}\{1+\alpha(x)\}\right].$$

Thus, $\Psi(x, r)$ is summarized as follows:

$$\Psi(x, r)=\delta^2\left\{\frac{1}{2}r^{*2}U_\infty+\psi_0(x, r^*)\right\}+\delta^4\psi_1(x, r^*)+\cdots\cdots\cdots\cdots\,.$$

5. Surface Pressure Coefficient

Using the above approximate solutions, each velocity component is expanded in a power series of δ shown below:

$$u=\delta u_1+\delta^3u_2+\cdots\cdots\cdots\cdots\,,$$

$$v=\delta r^*\omega \qquad \text{where, } \omega=O(1),$$

$$w=w_0+\delta^2w_1+\delta^4w_2+\cdots\cdots\cdots\cdots\,.$$

Then, the surface pressure coefficient C_p is expanded as

$$C_p=C_{p00}+\delta^2 C_{p11}+\delta^4 C_{p22}+\cdots\cdots\cdots\cdots,$$

where

$$C_{p00}=1-w_0^2,$$
$$C_{p11}=-(u_1^2+v^2+2w_0w_1),$$
$$C_{p22}=-(w_1^2+2w_0w_2+2u_1u_2).$$

Then, the first order approximation C_{p1} and the second order approximation C_{p2} to the surface pressure coefficient C_p are written as follows.

$$C_{p1}=C_{p00}+\delta^2 C_{p11}$$
$$C_{p2}=C_{p1}+\delta^4 C_{p22}$$

6. Numerical Calculations

In this paper, we consider a slender ellipsoid and a slender parabolic spindle given by $F(x)=\sqrt{1-x^2}$ and $F(x)=1-x^2$, respectively.

6.1. Flow patterns past a slender body

Flow patterns for the irrotational flow, the rotational flow with a paraboloidal velocity distribution and the swirling flow past a slender body are shown in Figs. 5, 6 and 7, respectively. Stream lines in the neighborhood of the front end of the body are shown interrupted for the parabolic spindle in Figs. 5 and 6, and for the

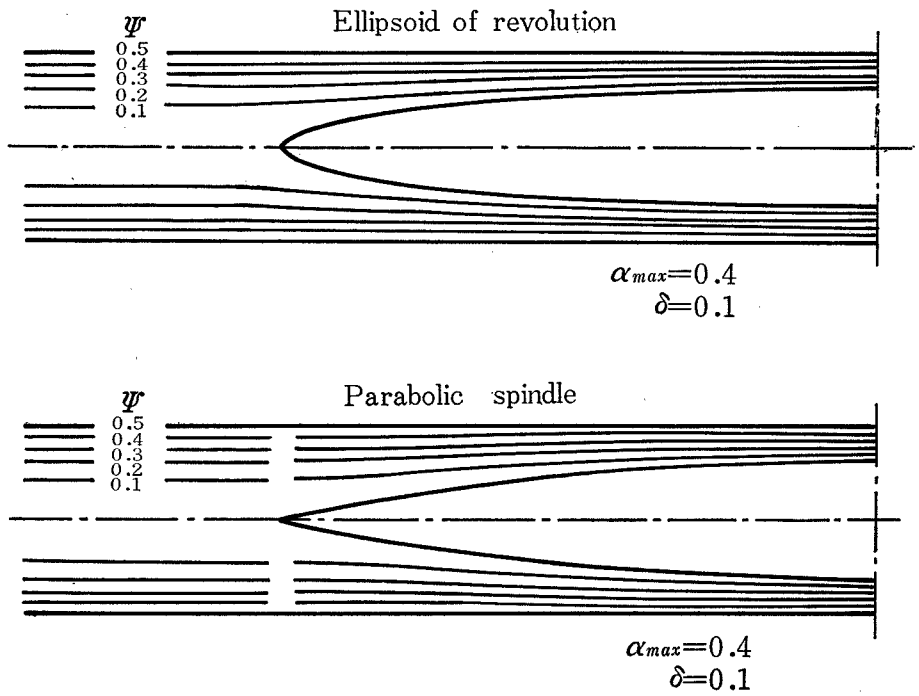

Fig. 5. Flow pattern for irrotational flow past a slender body of revolution in a tube

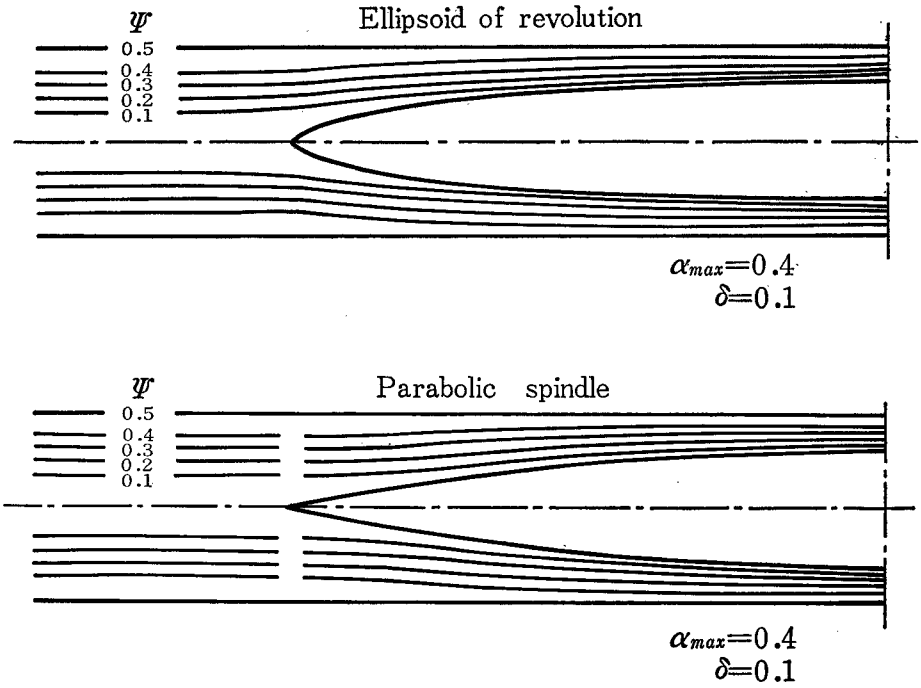

Fig. 6. Flow pattern for rotational flow past a slender body of revolution in a tube, upstream condition $w=W\left(1-\frac{r^2}{R_t^2}\right)$

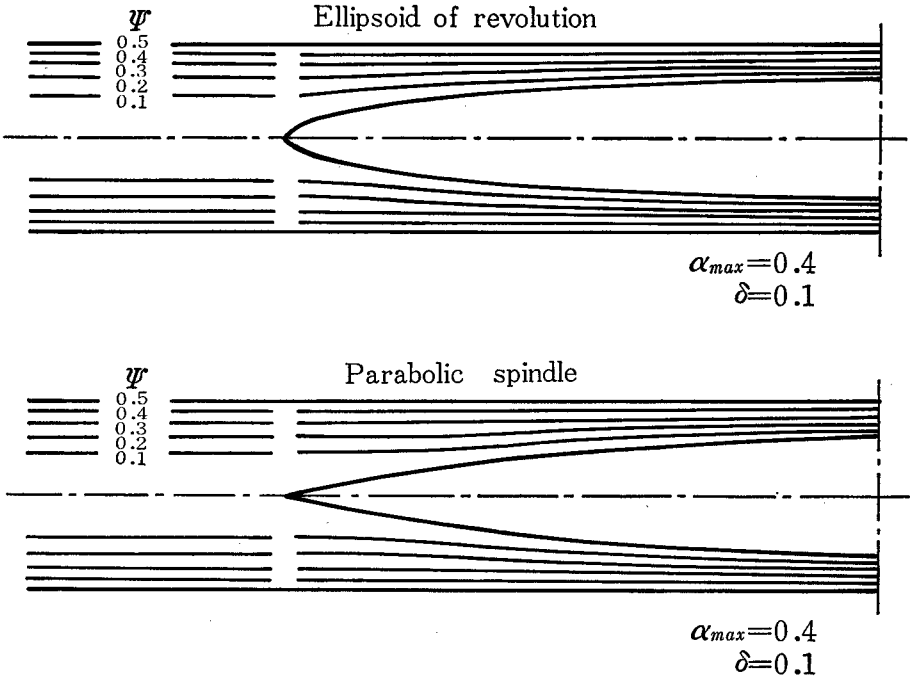

Fig. 7. Flow pattern for swirling flow past a slender body of revolution in a tube, Rossby number=1/3

ellipsoid and the parabolic spindle in Fig. 7, because this analysis is not valid in this region. However, stream lines in the neighborhood of the front end of the body are not shown interrupted for the ellipsoid in Figs. 5 and 6. For both the numerically calculated results[4] based on the distribution of the finite number of doublets and the present analytic results are shown for the ellipsoid in Figs. 5 and 6, and these results are graphically indistinguishable from each other.

From these flow patterns, it is revealed that stream lines become dense near the body and coarse near the tube wall for the irrotational flow. Stream lines in the swirling flow far upstream are denser near the tube wall than those in the irrotational flow.

6.2. Surface pressure distribution

Surface pressure distributions for the irrotational flow, the rotational flow and the swirling flow far upstream are shown in Figs. 8, 9 and 10. Broken lines are

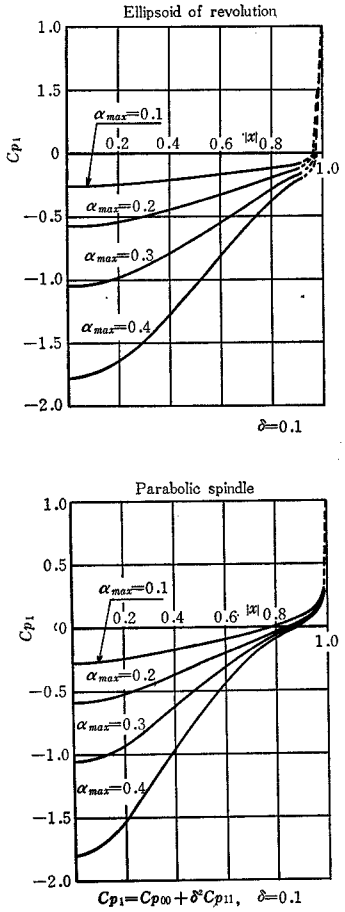

Fig. 8. Surface pressure distribution for irrotational flow past a slender body of revolution in a tube

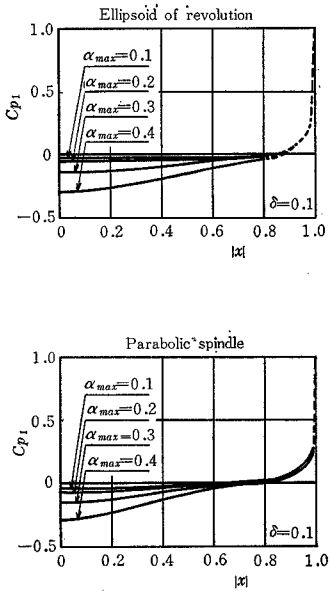

Fig. 9. Surface pressure distribution for rotational flow past a slener body of revolution in a tube, upstream condition $w=W\left(1-\frac{r^2}{R_t^2}\right)$

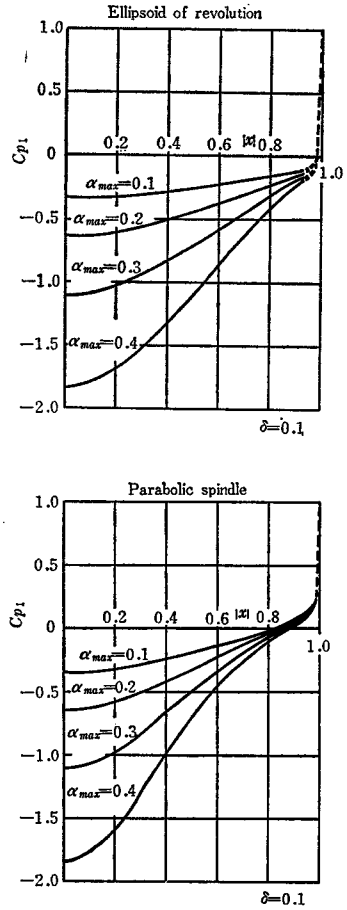

Fig. 10. Surface pressure distribution for swirling flow past a slender body of revolution in a tube, Rossby number=1/3

drawn outside the validity range of the present analysis in these figures. It can be seen that the surface pressure coefficients decrease as the blockage ratio α_{max} increases.

Since these surface pressure coefficients are normalized by the dynamic pressure on the axis of the tube, surface pressure coefficients for the rotational flow far upstream take larger values than those for the irrotational flow and the swirling flow far upstream. However, if surface pressure coefficients for the rotational flow are normalized by the dynamic pressure with the mean velocity, these values become four times as much as the values obtained in this analysis.

6.3. Effect for the reciprocal σ of a Rossby number

Surface pressure coefficients on the center cross section of the body in *case* 3 are shown against the reciprocal σ of a Rossby number in Fig. 11.

From this figure, the surface pressure coefficient in $\sigma=3$ decreases about 4 percent than that in $\sigma=0$ in both the blockage ratio α_{max} of 0.2 and 0.4.

6.4. Comparison of calculated results by this analysis with those by numerical method

The calculated results by the present analysis for *case* 1 and *case* 2 are compared in Fig. 12 with the numerically calculated result using a doublet distribution.

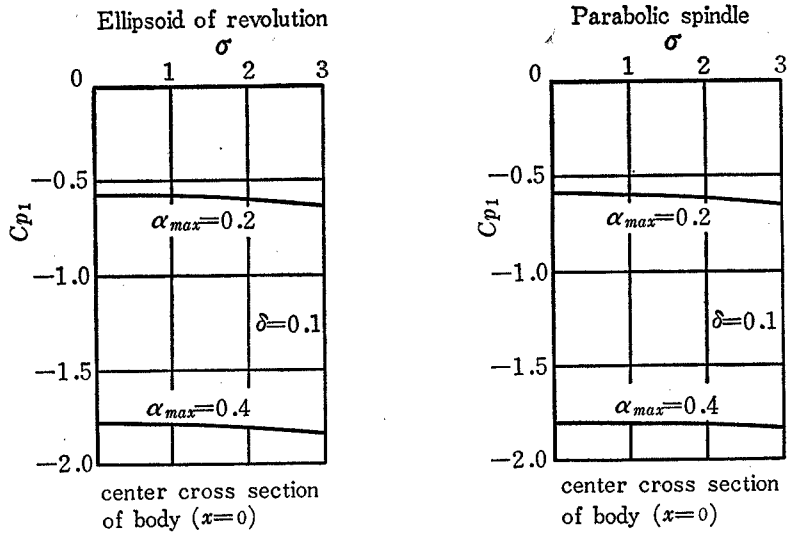

Fig. 11. Relation between surface pressure coefficient and reciprocal of a Rossby number for swirling flow

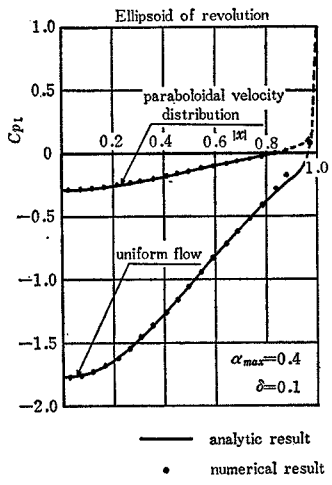

Fig. 12. Comparison of analytic results with numerical results for irrotational and rotational flow

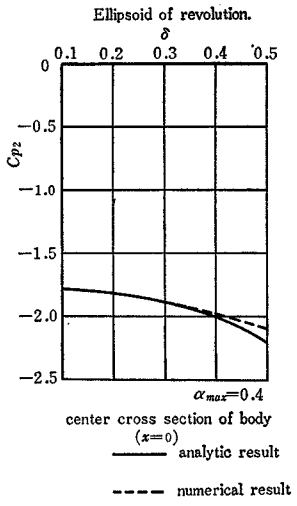

Fig. 13. Comparison of analytic results and numerical results for various values of slenderness ratio in the case of irrotational flow

These calculated results are graphically indistinguishable from each other in this figure. Therefore, the present analytic method can be used in practice.

6.5. Validity range of slenderness ratio δ

The calculated results using this analysis are varying the value of δ with the numerically calculated results for the ellipsoid of revolution in *case* 1 in Fig. 13.

It is shown from this figure that the present analytic method is valid up

to $\delta=0.35$. The surface pressure coefficient dereases as the slenderness ratio δ increases.

6.6. Validity of expansion in slenderness ratio δ

The first order approximation C_{P1} and the second order approximation C_{P2} to the surface pressure coefficient for the ellipsoid are shown in Table 1 for both the blockage ratio α_{max} of 0.2 and 0.4 in *case* 1.

From Table 1, a difference between the approximate surface pressure coefficients C_{P1} and C_{P2} in the case of $\delta=0.1$ can not almost recongnized. However, in the case of $\delta=0.3$, the second order approximation C_{P2} is smaller by 1 to 3 percent than the first order approximation C_{P1}.

Thus, the surface pressure coefficient C_P can be approximated by the first order approximation C_{P1} with good accuracy.

Table 1. Comparison between the first order approximation and the second order approximation of the surface pressure coefficients for slenderness ratio δ of 0.1 and 0.3 in the case of irrotational flow

Ellipsoid of revolution

α_{max}	δ	$\lvert x\rvert$	0.0	0.1	0.2	0.3	0.4	0.6	0.8
0.2	0.1	C_{P1}	−0.5744	−0.5667	−0.5440	−0.5072	−0.4581	−0.3318	−0.1895
		C_{P2}	−0.5747	−0.5670	−0.5442	−0.5074	−0.4583	−0.3320	−0.1898
0.2	0.3	C_{P1}	−0.6700	−0.6629	−0.6421	−0.6088	−0.5656	−0.4655	−0.4162
		C_{P2}	−0.6910	−0.6836	−0.6621	−0.6278	−0.5833	−0.4808	−0.4348
0.4	0.1	C_{P1}	−1.7883	−1.7516	−1.6459	−1.4828	−1.2789	−0.8192	−0.3864
		C_{P2}	−1.7886	−1.7519	−1.6461	−1.4830	−1.2791	−0.8192	−0.3861
0.4	0.3	C_{P1}	−1.8724	−1.8357	−1.7300	−1.5676	−1.3657	−0.9207	−0.5596
		C_{P2}	−1.8946	−1.8570	−1.7486	−1.5822	−1.3755	−0.9200	−0.5382

$C_{P1}=C_{P00}+\delta^2 C_{P11}$, $C_{P2}=C_{P1}+\delta^4 C_{P22}$

7. Conclusions

A rotational and an irrotational flow past a slender body of revolution located on the axis of an infinitely long tube of constant diameter is analyzed using the slender body in slender tube theory and a comparison is made between these analytic results and other numerical results calculated from the distribution of the finite number of doublets.

Following conclusions are obtained;

(1) The solution is more easily obtained using the method of the present analysis than using the numerical method.

(2) The validity range of the slenderness ratio δ is up to 0.35 in the present analysis.

(3) It will be sufficient for the surface pressure coefficient to be obtained using the

first order approximation C_{P1}.

(4) The surface pressure coefficient decreases as the blockage ratio, the slenderness ratio or the reciprocal of a Rossby number increases.

(5) Values of the surface pressure coefficient for various far upstream conditions become small in order of the rotational flow with a paraboloidal velocity distribution, the irrotational flow and the swirling flow, respectively.

References

1) Wei Lai, J. Fluid Mech., **18**, 587 (1964).
2) G.K. Batchelor, An Introduction to Fluid Dynamics, Cambridge at the University Press, (1967).
3) J.D. Cole, Perturbation Methods in Applied Mathematics, Blaisdell Publishing, (1968).
4) C. Tojo and H. Nakatani, Bull. Univ. Osaka Prefecture, Ser. A, 21, **1**, 1 (1972).
5) P. Levine, J. Aero/Sci., **25**, 33 (1958).